Smart Agricultural Technology 13 (2026) 101708

Contents lists available at ScienceDirect

Smart Agricultural Technology

journal homepage: www.journals.elsevier.com/smart-agricultural-technology

Machine learning models for actual crop coefficient estimation on sensor-less fields

Federico Amato [a], Matteo Ippolito [a], Dario De Caro [a], Daniele Croce [a,b], Antonino Pagano [a,b,*]

[a] Department of Engineering, University of Palermo, Viale delle Scienze, Building 9, 90128 Palermo, Italy
[b] CNIT - Consorzio Nazionale Interuniversitario per le Telecomunicazioni, Parma, Italy

ARTICLE INFO

Keywords:
Actual crop coefficient
Machine learning
Water management
ERA5-L
Random forest
Sustainable agriculture

ABSTRACT

Efficient freshwater management in agriculture is a critical global priority due to increasing pressures from climate change and a growing population. Irrigated agriculture, which accounts for 70% of global freshwater withdrawals, plays a vital role in food security but faces significant challenges due to water scarcity and changing climatic conditions. In this context, accurate estimation of the actual crop coefficient (K_{c-act}) is essential to optimise irrigation strategies, thus improving water use efficiency, and enhancing the resilience of agricultural systems. This study proposes an innovative machine learning framework to estimate K_{c-act} across different temperate and continental climatic zones, without relying on field sensors. By integrating ERA5-L reanalysis data, the model provides accurate K_{c-act} estimates even in the absence of complete datasets. The framework was tested on a wide range of crops, including both homogeneous herbaceous crops (e.g., wheat and maize) and tree crops (e.g., citrus and olives), demonstrating its adaptability to different agricultural contexts. The process includes data preprocessing, actual evapotranspiration (ET_a) prediction (using a Random Forest model), and seasonal decomposition to regularise the data. Results demonstrate significant accuracy improvements over traditional methods, with RMSE values as low as 0.073 for citrus orchards and 0.143 for olive groves. The analysis reveals variations in the values K_{c-act} influenced by climatic and field management conditions, offering a practical tool to optimise irrigation strategies and improve the efficiency of water use. The model reduces the dependency on expensive equipment and provides a scalable solution to monitor and manage water resources in agriculture.

1. Introduction

The optimization of freshwater resource management in agriculture is of pivotal importance. Indeed, freshwater sustainable management has become a global priority to address mounting challenges, such as climate changes and the rising of global population. In fact, climate changes, with its profound impact on precipitation patterns and freshwater availability, have intensified the need to safeguard this essential resource. Simultaneously, the rising global population [21] is driving an unprecedented demand for food, further increasing pressure on freshwater resources, particularly those used for irrigation, which accounts for 70% of freshwater withdrawals worldwide [77]. In this context, ensuring the efficient and equitable use of freshwater for agricultural purposes is crucial. Irrigated agriculture plays a key role in global food security, but is increasingly vulnerable to freshwater scarcity. Addressing this challenge requires innovative strategies to optimise water use, minimise waste, retrieve reliable estimation of crop water needs, and enhance agricultural systems resilience to changing climatic conditions.

One of the key tools for this management is the correct estimation of crop coefficient in real soil conditions ($K_{c-act} = K_c \cdot K_s$), hereafter named the actual crop coefficient. This coefficient enables the evaluation of actual crop evapotranspiration (ET_a), taking into account possible stress conditions due to the insufficient soil water content. According to the FAO-56 single crop coefficient approach [7], the actual crop coefficient (K_{c-act}) could be retrieved through the ratio between actual evapotranspiration (ET_a) and the crop reference evapotranspiration (ET_o):

$$K_{c-act} = K_c \cdot K_s = \frac{ET_a}{ET_o} \tag{1}$$

The crop coefficient (K_c) reflects the morphological and eco-physiological characteristics of the crop, as well as cultivation techniques, phenological phases, and soil coverage. Its value is strongly influenced by the environmental conditions of the plant's growth area. Thus, K_{c-act} is specific to each crop and varies seasonally and annually due to changes in the crop's morphological and eco-physiological characteristics over time [51]. As K_c depends on the crop's growth stage,

* Corresponding author.
E-mail address: antonino.pagano@unipa.it (A. Pagano).

https://doi.org/10.1016/j.atech.2025.101708
Received 4 August 2025; Received in revised form 6 November 2025; Accepted 9 December 2025
Available online 26 December 2025
2772-3755/© 2025 The Author(s). Published by Elsevier B.V. This is an open access article under the CC BY license (http://creativecommons.org/licenses/by/4.0/).

it is essential to use distinct values for different phenological phases [7]. Traditionally, K_c is defined through trapezoidal time series specific for each crops [7,62].

The stress coefficient (K_s), expression of the actual crop water stress conditions, is typically calculated as a function of the soil water content within the root zone [7,72].

Actual evapotranspiration (ET_a) can be measured and estimated using various methods, each with unique advantages and limitations. For example, lysimeters provide direct and highly accurate measurements by isolating a volume of soil and vegetation, allowing precise water balance calculations [67]. Eddy covariance towers [37,65,73], on the other hand, measure the flux of water vapor in the atmosphere above the canopy, offering high temporal resolution data and valuable insights into ecosystem-scale processes [16,76,86]. Moreover, the AmeriFlux platform provides high-quality data on ET_a derived from energy and water flux measurements across diverse ecosystems, enabling accurate field-level assessments. AmeriFlux is a research network that measures carbon, water, and energy exchanges across various ecosystems in the Americas, providing critical data to analyse ecosystem responses to climate variability and land-use changes, which support the global carbon cycle and climate modeling. In addition to these traditional methods, remote sensing (RS) has emerged as a powerful tool for estimating ET_a over large spatial scales. Using multi-platform satellite or airborne data, characterised by good spatial and temporal resolution, RS techniques can capture surface energy balance components [15], vegetation indices [35], and land surface temperatures [9], allowing the estimation of ET_a in a distributed way, across diverse landscapes. Machine learning (ML) models further enhance this capability by integrating large datasets from ground measurements, remote sensing inputs, and meteorological variables to predict evapotranspiration with high spatial and temporal precision [19,28,29,52]. These approaches, combined with traditional methods, provide scalable solutions for monitoring water use and managing agricultural resources.

1.1. Background and outstanding issues

According to the commonly used Penman-Monteith (PM) equation [7], ET_o represents the atmospheric evaporative demand, calculated using only agro-meteorological variables considering hypothetical reference crop characteristics. These variables can be measured directly by standard weather stations and sensors installed in the fields, or provided by reanalysis databases.

Reanalysis datasets, derived from data assimilation techniques, are among the most widely used resources to study climate dynamics [53]. The reanalysis method combines model outputs with global historical observations to monitor and forecast climate change, supporting applications in research, education, and industry. Several gridded reanalysis climate data products have been developed, with different spatial and temporal resolutions, and are made freely available by research institutions such as the National Aeronautics and Space Administration (NASA) and the European Centre for Medium-Range Weather Forecasts (ECMWF). These global datasets, providing atmospheric and land surface variables, are represented as 'gap-free maps' that combine weather forecast models with data assimilation systems, regularly 'reanalysed' using historical observations. In 2019, ECMWF released the ERA5-Land (ERA5-L) product, an evolution of the ERA5 dataset, designed to enhance spatial resolution to a 0.1° latitude by 0.1° longitude grid. In ERA5-L, land surface simulations are driven by atmospheric forcing variables such as air temperature, humidity, and pressure. More details on the model used to produce ERA5-L can be found in the IFS Documentation CY45R1 (IFS Documentation CY45R1, ECMWF, 2018). With its advanced spatial and temporal resolution, ERA5-Land provides a comprehensive range of meteorological data on a global scale, making it an ideal resource for capturing actual hydrological conditions. Therefore, to estimate and map crop coefficients globally, reliable, near-continuous meteorological information that is both time-sensitive and spatially distributed is essential.

In the literature, many studies have shown that reanalysis climate data generally provides a good approximation of data recorded by climate stations [50,56,70]. Specifically, the suitability of ERA5-L databases for estimating various climate variables has been recently evaluated by multiple authors [8,19,33,57,58,79]. Moreover, [27,79] and [33] obtained reliable and encouraging ET_o estimations without implementing a bias correction procedure. Importantly, these datasets are easily accessible through the Google Earth Engine (GEE) platform, which enables streamlined data retrieval, processing, and integration. This accessibility significantly reduces the computational burden and technical barriers often associated with handling large-scale reanalysis datasets, making data processing more efficient. GEE enables the rapid processing of extensive RS datasets through cloud computing resources, which users can access via an Internet connection [26].

1.2. Contributions of the work

This study proposes the development of an innovative ML framework that integrates reanalysis data from ERA5-L with ET_a data from the Eddy covariance towers to provide more accurate estimations of K_{c-act}. In particular, the primary goal of the models developed in this study is to enhance the accuracy of actual crop coefficient estimations across different climatic zones and agronomic contexts, offering a tool that considers the interactions between the water cycle, crops, and meteorological conditions. The outcomes aim to provide a robust foundation for more efficient irrigation strategies, with significant implications for sustainability and food security. The decision to utilise reanalysis data was driven by the aim to develop an accessible ML model capable of estimating actual crop coefficients without relying on field sensor measurements. Field sensors often require continuous maintenance, can still suffer from data gaps, and, in some cases, may also involve significant costs. Indeed, the Eddy covariance data is used only for training: then, the proposed ML framework alone provides a good estimate of the actual crop coefficient.

The process of the proposed framework consists of different steps: initially, the data is pre-processed by imputing missing data and rescaling the features. Then, the Random Forest model is trained to predict ET_a values by selecting the best model through cross-validation. The daily values of K_{c-act} are subsequently calculated as the ratio of ET_a to ET_o. A post-processing step removes outliers from the K_c series. Finally, the seasonal decomposition algorithm and outlier removal regularise the series, before comparing the average values of the reconstructed series with the theoretical baseline models for each season.

The framework was tested on a wide range of crops, including both homogeneous herbaceous crops (e.g., wheat and maize) and tree crops (e.g., citrus and olives), demonstrating its adaptability to different agricultural contexts. The results obtained show significant improvements over traditional methods, with RMSE values as low as 0.073 for citrus orchards and 0.143 for olive groves.

The primary objective of this study is the development of models based on the seasonal decomposition process, aimed at improving the accuracy of crop coefficient estimates and, consequently, refining the assessment of irrigation water consumption. These models are designed to optimize water resource management in agriculture, by integrally considering the interactions among the water cycle, crops, and meteorological conditions across different climatic and agronomic contexts.

2. Materials and methods

2.1. Experimental fields

The experiment was conducted across six different fields: two located in Italy, three in USA, and one in Canada (Fig. 1). Table 1 provides a comprehensive overview of the experimental fields included in this

Table 1
Experimental fields with their crops, geographical coordinates, climatic zones, and analysis periods.

Field	Extension [ha]	Main crop	Latitude	Longitude	Climatic zone	Analysis period
Villabate	0.50	Citrus	38°4’53.4”N	38°4’53.4”E	Csa	2019-2023
Castelvetrano	6.00	Olives	37°38’61”N	12°50’53”E	Csa	2009-2011
US-ARM	13.00	Winter wheat	36°3620.9”N	97°29’19.59”O	Cfa	2005-2010
US-Ne1	50.00	Maize	41°09’54.56”N	96°28’35.50”O	Dfa	2001-2020
US-CF1	40.00	Winter wheat	46°46’53.53”N	117°4’55.50”O	Dsb	2018-2020
CA-ER1	13.00	Maize	43°38’26.17”N	80°24”44.35”O	Dfb	2016-2019

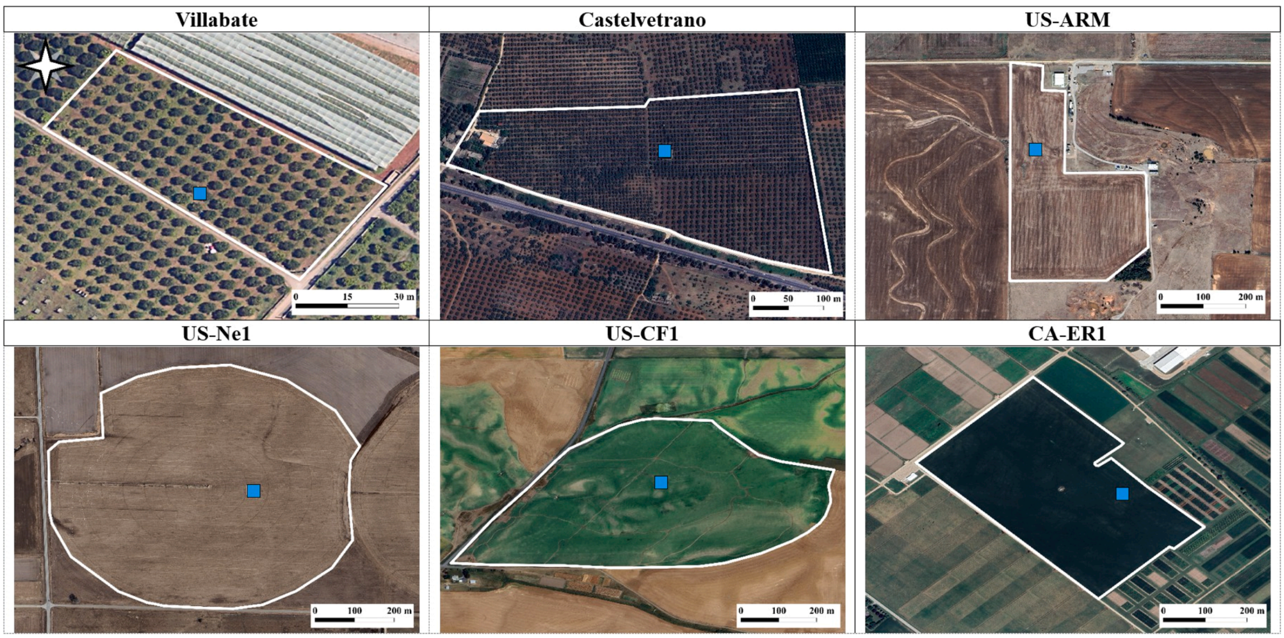

Fig. 1. Experimental fields; the blue squares indicate the Eddy covariance towers position.

study, detailing their respective crops and analysis periods. The fields span a wide range of latitudes and longitudes, encompassing various climatic zones.

2.1.1. Fields in Italy

The first field (Villabate) is a 0.50 *ha* Mediterranean citrus orchard (Citrus reticulata Blanco, cv. Mandarino Tardivo di Ciaculli), located near Palermo, Italy (38° 4’ 53.4” N, 13° 25’ 8.2” E). The field can be classified as having a low plant density [7,62]. Experimental activities were carried out here from 2019 to 2023. Additional information regarding the experimental setup, field and crop characteristics can be found in [35].

The second field (Castelvetrano) is an olive orchard with the “Nocellara del Belice” variety which spans approximately 6.00 *ha*. This field is located in southwestern Sicily, Italy (37°38’61” N, 12°50’53” E), about 5 km from the town of Castelvetrano, and is part of an irrigation district characterised by flat terrain and uniform soil and crop types. The field can be classified as having a traditional, medium plant density [7,62]. The experimental activities at this location were conducted over three years, from 2009 to 2011. More details on this field and crop characteristics are provided by [63]. According to the latest version of the Köppen climate classification, both Italian fields exhibit a Hot-summer Mediterranean climate (Csa) [39], characterised by rainfall predominantly occurring in the fall and winter, with hot and dry summers.

2.1.2. Fields in USA and Canada

The American and Canadian sites, differ in cultivation and climate classification. The third site (US-ARM) of about 13.00 *ha* is located near Billings, Oklahoma, USA (36° 36’ 20.9”N, 97° 29’ 19.59” W). The primary crop is hard red winter wheat (Triticum aestivum L., mainly var. Jaeger, Jagalene, and Fuller), with occasional crop rotations [23,64]. Experimental activities took place here from 2005 to 2010. The climate, based on the Köppen classification [39], is Humid subtropical (Cfa). The fourth site (US-Ne1) of about 50.00 *ha* is situated near Mead, Nebraska, USA (41°09’ 54.56”N, 96° 28’ 35.50” W). This field employs a center pivot irrigation system and has a ten-year history of maize-soybean rotation under no-till practices [75]. The experimental period spanned from 2001 to 2020. The Köppen classification [39] identifies the climate as Hot-summer humid continental (Dfa). The fifth site (US-CF1) of about 40.00 *ha*, located near Pullman, Washington, USA (46° 46’ 53.53”N, 117° 4’ 55.50” W), primarily grows winter wheat, spring cereals (barley and wheat), and pulse crops (dry pea, lentil, and chickpea) [47]. Experimental activities were conducted from January 2018 to December 2020. According to the Köppen classification [39], this region has a Warm, dry-summer continental climate (Dsb). The sixth site (CA-ER1) of about 13.00 *ha* is located near Guelph, Ontario, Canada (43°38’26.17”N, 80° 24’ 44.35” W), where maize is the main crop. The terrain is relatively flat and homogeneous [82]. Experimental activities on this site were performed from 2016 to 2019. Based on the Köppen classification [39], the climate is classified as Warm-summer humid continental (Dfb).

The analysis periods for these fields vary significantly, ranging from 2001 to 2020, with a minimum duration of 3 years for Villabate and Castelvetrano and a maximum of 20 years for US-Ne1. This wide temporal range validates the study on data collected in both long and short terms, allowing for a more comprehensive evaluation of crop performance in different environments.

2.2. Micrometeorological data

Micrometeorological data were obtained from Eddy Covariance towers for the Italian orchards, and from the AmeriFlux network (AMERIFLUX, https://ameriflux.lbl.gov) for the orchards in Canada and the USA.

2.2.1. Heat flux datasets

In both Italian experimental fields, actual evapotranspiration (ET_a) was estimated using an Eddy Covariance (EC) flux tower. Further details about the EC tower equipment in the citrus and olive orchards can be found in [35] and [16], respectively. Sensible, $H\,[W m^{-2}]$, and latent, $LE\,[W m^{-2}]$, heat fluxes were evaluated as:

$$H = \rho c_p \sigma_{WT} \tag{2}$$

$$\lambda ET = \lambda \sigma_{WQ} \tag{3}$$

where $\rho\,[g m^{-3}]$ is the air density, $c_p\,[J g^{-1} K^{-1}]$ is the air specific heat capacity at constant pressure, $\sigma_{WT}\,[m K s^{-1}]$ is the covariance between vertical wind speed and air temperature, $\lambda\,[J g^{-1}]$ is the latent heat of vaporization and $\sigma_{WQ}\,[g m^{-2} s^{-1}]$ is the covariance between vertical wind speed and the water vapor density, respectively. All the fluxes were evaluated, using Eqs. (2) and (3), with a time step of 30 min using the software developed by [45]. All the fluxes at the half hourly time steps were then aggregated at the daily time step.

Latent heat flux (LE) values for the American and Canadian sites were retrieved by the AmeriFlux BASE data product. Data from three of the sites were available at a half-hourly resolution, while the US-Ne1 site provided data at an hourly resolution [12,59,74,82]. The data, shared under a CC-BY-4.0 license, were downloaded, and the LE values at both half-hourly and hourly intervals were aggregated to a daily time step.

2.2.2. Quality assurance and quality control

For the Italian field, the raw EC data were post-processed following the procedure outlined by [45], which closely aligns with the FLUXNET standard protocol [46,54,55]. Data de-trending was carried out using a running mean, and a coordinate rotation was applied to the sonic anemometer data to achieve zero mean vertical and transversal wind speeds. Corrections for spectral loss were also performed. Additionally, adjustments were made for high wind speeds affecting sonic temperature, and the Webb-Pearman-Leuning corrections were applied for water vapor [48] before the final calculation of half-hourly fluxes. Finally, all records from days with rainfall exceeding 2.5 mm were excluded. Such exclusion is standard for Eddy covariance measurements, as precipitation can compromise the accuracy of vertical turbulent flux readings. Rainfall introduces noise and distorts evapotranspiration estimates by causing water accumulation on sensors and temporary surface evaporation, which do not represent natural atmospheric fluxes [10,81]. The method suggested by [60], based on the Closure Ratio (CR), was used to assess the surface energy balance closure. When the energy storage in the soil is neglected, CR represents the slope of the regression line between the available energy given by the variance of the net radiation, R_n, and the soil heat flux, G, and the covariance of the turbulent heat fluxes ($LE + H$) only evaluated from the subset of half hourly data corresponding to $R_n \geq 100\ W m^{-2}$:

$$CR = \frac{LE + H}{R_n - G} \tag{4}$$

For the citrus orchard, the values of CR were equal to 0.98, 0.88, 1.03, and 0.88 for 2019 [35], 2020 [35], 2021 [52], and 2022 [52], respectively. On the other hand, for the olive orchard, the values of CR were equal to 0.90 for 2009 [16], 0.92 for 2010 [16], and 1.02 for 2011 [9].

Fig. 2 shows the relationships between the turbulent heat fluxes ($H + LE$) versus the available energy ($R_n - G$) measured by the EC tower installed in the citrus field, in 2023. The corresponding CR is equal to 0.94. [41] deemed acceptable CR values to range between 0.80 and 0.90 for tree crops. However, higher CR values of 1.08 and 1.03 were reported by [22] in two citrus orchards located in southern Morocco, which are characterised by a semi-arid Mediterranean climate. The CR estimates for the two fields in this study align with values reported in the literature and are therefore considered reliable.

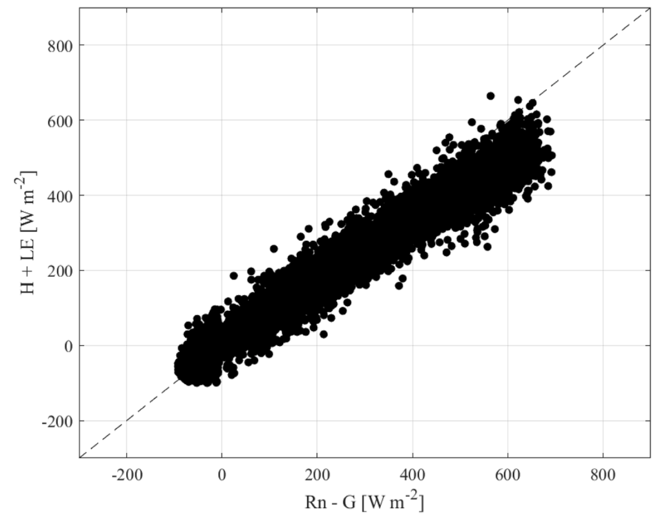

Fig. 2. Relationships between turbulent heat fluxes, $H + LE$, and available energy, $Rn - G$, measured by the EC tower in 2023.

The Quality Assurance (QA) and Quality Control (QC) of the AmeriFlux BASE data adhere to the methodology used for processing the FLUXNET2015 dataset [54]. Each site's data undergoes QA and QC steps specifically tailored for generating these derived data products. Several of these QA and QC procedures are detailed in [55], which includes a processing flowchart outlining all the applied steps. The QA and QC processes involve evaluating units and sign conventions, timestamp alignment, trends, step changes, and outliers based on site-specific historical ranges, as well as multivariate comparisons, diurnal/seasonal patterns, friction velocity filtering, and variable availability. Quality checks are performed on individual variables, combinations of variables, or through more specialised tests. Finally, only the days with 48 half-hourly measurements were used in the experiment, to guarantee the consistency of the daily data.

2.3. Reanalysis data

For all the six fields, daily reanalysis data of maximum and minimum air temperature, T_{max} and T_{min} [°C], global solar radiation, $R_s\,[W m^{-2}]$, dew-point temperature, $Tdew$ [°C], and the two components, eastward and northward, of wind speed measured at 10 m above the ground, U_{wind} and $V_{wind}\,[m s^{-1}]$, were downloaded using the ERA5-Land Daily Aggregated - ECMWF Climate Reanalysis dataset, available in the Google Earth Engine (GEE) platform (ECMWF/ERA5-LAND/DAILY-AGGR, https://developers.google.com/earth-engine/datasets/catalog/ECMWF_ERA5_LAND_DAILY_AGGR). The ERA5-Land last generation of the global reanalysis climate database, provided by the European Centre for Medium-Range Weather Forecasts (ECMWF), is freely downloadable from the internet and is characterized by a spatial resolution of 0.10° latitude and 0.10° longitude and a temporal coverage from 1950 up to five days before the real-time. Global datasets of atmospheric and land surface variables, represented in 'maps without gaps', are created coupling weather forecast models and data assimilation systems, periodically reanalysed' by past observations. The reanalysis method combines model data based on past observations across the world for monitoring and forecasting climate change, for research, education, and commercial applications. GEE is a cloud-based platform designed for geospatial visualization and analysis of large-scale datasets at a planetary level. It

Table 2
Hyperparameters and their corresponding ranges of RF grid search.

Hyper Parameter	Range
Estimators (number of decision trees)	100 to 1000 (steps of 100)
Max depth	None, or 10 to 50 (steps of 10)
Minimum samples split	2 to 20 (steps of 2)
Minimum samples leaf	1, 2, 4
Bootstrap	True, False
k-folds for cross validation	3 to 10 (steps of 1)

is freely accessible to academic, non-profit, business, and government users. By leveraging cloud computing technologies, GEE effectively addresses the challenges of managing and processing big data, offering an innovative approach to handle remote sensing information.

The quality of ERA5-Land data was assessed through direct comparisons with numerous in situ observations, primarily collected between 2001 and 2018, as well as by comparing it with other model-based or satellite-derived global reference datasets [66]. A comparison between ground-based and reanalysis data was conducted by [19] in the citrus orchard and [33] in the olives orchard. These studies, carried out in citrus and olive orchards where both datasets were available, enabled an assessment of the suitability of reanalysis climate variables in cases where ground data are unavailable.

2.4. The random forest machine learning model

A Random Forest is a collection of random trees [13]. Specifically, Decision Trees are ML algorithms usually chosen for the simplicity of their approach and visual representation: starting from the complete set of features, each branch of the tree selects a feature and tries to classify the data point with respect to the target classes [14]. If a classification is possible, the branch ends in a leaf labelled by a specific class or a probability distribution among the classes. If the classification is not yet possible, the branch continues to a new branch with a new feature.

To avoid overfitting training data, more trees are used with the bootstrap aggregating technique, selecting a random sample and replacing the training set to fit the trees, so that no tree is trained with the complete set of data. More randomness is given selecting only a random subset of candidate features for each branch split. The final output is given then by majority voting among the output of each tree. In addition, to calculate the optimal values of the hyperparameters, the grid search technique was applied. The performance of the model was evaluated using the different combinations of parameters as listed in Table 2. The best set of hyperparameters identified for each field is presented in the results Section 5.

2.5. Statistical evaluation metrics

To validate the proposed K_{c-act} framework, multiple statistical metrics were used to assess the accuracy and precision of the predictions. The Root Mean Squared Error (RMSE) measures the mean square deviation between observed and predicted values, providing an indication of the absolute accuracy of the model [17]. The normalised version, nRMSE, expresses the RMSE as a percentage of the observed mean, facilitating comparison between different datasets [87]. The Mean Bias Error (MBE) calculates the mean difference between observed and predicted values, indicating any over- or underestimation trends [84]. The Mean Absolute Error (MAE) represents the mean absolute error, ignoring the sign, to provide a more robust measure of accuracy [84]. Moreover, the percent bias (PBIAS) quantifies the relative tendency of the model with respect to observed values, highlighting any systematic bias [49]. Finally, we can compare the trapezoid models with the values of K_{c-act} actually measured and quantify the improvement in the representative power of our values with respect to the more general reference models. To define the relative Accuracy Improvement we compute the root mean squared error for all trapezoidal models of K_{c-act} with respect to the Eddy covariance measures of K_{c-act}, to get the average error linked to each model, E_{model}. We then compare the difference between the errors of reference models with the RMSE of our model and take the ratio with E_{model}.:

$$\text{Improvement} = \frac{E_{\text{model}} - \tilde{E}}{E_{\text{model}}} \tag{5}$$

where $\tilde{E}$ is our model's error and the reference model can be one of: *FAO-56*, *FAO-56-fs*, *FAO-56-nfs*, *FAO-56-mg*, *FAO-56-ms* or *Rallo*, to be explained later in Section 3.5. With this definition, a positive improvement means that our model provides a reduction in the average distance between the measured data and the estimated K_{c-act} value, vice versa for negative values. An Improvement of 50% means the error is halved using our model and the limit value 100% implies that the RMSE between our model and the data is zero.

3. Framework description

This section describes the ML framework, the pre-training process to perform gap-filling on the ET_a time series, the K_{c-act} time series calculation, the post-processing and seasonal decomposition. The Algorithm 1 represents the pseudocode to estimate the dynamics of K_{c-act} during the observation period. The structure of the code comprises six main blocks, illustrated in detail in the following subsections.

3.1. Pre-processing

Pre-processing data is critical during this phase to increase the model performance. Missing data were first imputed using an iterative imputation approach and then standardised. Iterative imputation uses a multivariate imputer to estimate each feature based on all other features. The method involves modelling each missing value as a function of other features in a round-robin form [78]. In addition, the standard-scaler, or z-score, [1] is used to organise the data into a standard normal distribution with zero mean and unit variance. In this manner, all input features were normalised and scaled to have a comparable range. This is important to speed up and improve convergence in training, as well as for assigning equal weights to all the features. Finally, time series are shuffled to reduce over-fitting and generalise the models.

3.2. Gap filling in ET_a time series using RF model

The number of daily ET_a measurements for each field is summarised in Table 3. For each field, it is also possible to observe the percentage of missing data. For example, in the Villabate field, the percentage of missing data is 46.3% of the total days in the monitoring period. These missing data were caused by the malfunctioning of the installed instruments. For this reason, the RF model can be used not only to predict new values in future periods but also to fill in the gaps in the time series of ET_a. In particular, in this step of the algorithm, RF machine learning models were trained and their performance was evaluated using cross-validation [38].

3.3. Post-processing

At this point, the developed model was used to determine the trend of the crop coefficient for the years of observation. In particular, Eq. (1) was used to derive the $(K_c \cdot K_s)$ time series for the examined crop. Subsequently, an automatic outlier detection model called Isolation Forest [42], which is a tree-based anomaly detection algorithm, was applied to remove outliers in the K_{c-act} time series.

Algorithm 1: Framework to estimate K_{c-act} dynamics. All the functions below are to be run one after the other.

Input: n measures of m accessible features F and $n-y$ measures of the target ET_a in the same days
Result: n days of crop coefficient K_c values, both measured and synthetic

```
function preprocess_data():
    Read input data F and ET_a ;
    Impute missing data in F ;
    Extract the set Y ∈ ℝ^{y×m+1} where the target is unknown ;
    Take the set X ∈ ℝ^{x×m+1} of data for which we have target
      measures;
    Randomize X and create n_k folds of X_train and X_test ;
    Regularize separately test and training data for each fold ;
function make_model(model_parameters):
    /* training loop with cross-validation                 */
    for k in range(n_k) :
        Train model on X_train ;
        Compute the R^2 score using X_test and save it ;
    Save best-performing model
function predict_ETa():
    /* model creation and fine-tuning                      */
    Choose a ML model ;
    Optimize the model with a grid search over its parameters ;
    Using the best trained model make predictions for Y's
      target values ;
    Append predictions to the measures and rescale data back
      to their original range ;
    Compute the the crop coefficient as ET_a/ET_o from ET_a
      measured and synthetic data ;
function postprocess_Kc():
    Remove outliers and noise from the seasonal
      decomposition of K_c ;
function make_seasonal_Kc():
    Take standard values of K_c per season ; // Given for
      example in Allen et al., 2009
    Compare average values of the reconstructed K_C series
      with tabular data ;
```

Table 3
Data Summary with Missing Data Percentage in ET_a time series for different fields.

Field	Observation Days	Measurement Days	Missing Data [%]
Villabate	933	501	46.3
Castelvetrano	1095	573	47.7
US-ARM	2191	1858	15.2
US-Ne1	7305	6512	10.9
US-CF1	1096	809	26.2
CA-ER1	1461	1160	20.6

3.4. Seasonal decomposition

The ET_a/ET_o ratio has a significant seasonal component that effects the K_{c-act} time series. Under certain conditions (particularly hot summers, high water stress, presence of weeds, etc.), the time series may exhibit significant dispersion. To create a reliable K_{c-act} time series, the ET_a/ET_o ratio was divided into three additive components: average trend, seasonality, and residual. The statsmodels Python program [68] is used to obtain the decomposition, which is based on a convolution filter and moving average. This allows for the easy removal of the residual (or noise). Then, by combining the other two components (average trend and seasonality), dispersion in the time series can be reduced. By analysing the residuals, it is observed that their distribution is approximately Gaussian and zero-centered, as discussed in Section 5 (Fig. 7). This characterization as Gaussian noise supports the removal of this component.

3.5. Evaluation

The last step consists of evaluating the K_{c-act} values estimated by the framework according to the metrics presented in Section 2.5. Specifically, the results obtained are compared against various K_c theoretical trapezoidal models [7,62]. These models are realised considering the lengths of crop phenological stages for various planting periods and climatic regions. The comparison between the actual and theoretical crop coefficients was adopted in this study to ensure a replicable approach based on established data. While this methodology has the limitation of not providing a direct and dynamic estimation of the water stress coefficient, it represents a practical solution in the absence of specific measurements and allows for robust and comparable preliminary evaluations within the proposed framework. However, a simple preliminary evaluation was performed by estimating K_s as the ratio between the K_{c-act}, obtained applying the ML framework, and the corresponding theoretical trapezoidal K_c, as suggested by the inverted Eq. (1). This approach offers an indirect evaluation of potential water stress conditions and enables a qualitative assessment of model performance across different environmental settings, considereing the lack of field measurements for direct validation.

The homogeneous crops, winter wheat (US-ARM and US-CF1) and maize (US-Ne1 and CA-ER1), were compared with two theoretical models suggested by [7]. For winter wheat (US-ARM and US-CF1), one model (FAO-56-fs) considers the possibility of frozen soil during the crop growth stages, while the other (FAO-56-nfs) assumes its absence. For both models, the K_c values take into account the possibility that the winter wheat is hand-harvested. For maize (US-Ne1 and CA-ER1), the first model (FAO-56-mg) accounts for grain maize growth stages, whereas the second (FAO-56-ms) addresses sweet maize stages.

Instead, the tree crops (Villabate and Castelvetrano) were compared with two theoretical models suggested by [7] and [62]. The models are different because the first (FAO-56) considers the presence of ground weeds, while the second (Rallo) their absence. The use of specific theoretical models for each crop is justified by the lack of precise knowledge regarding the management characteristics of the analysed fields. This approach allows for greater flexibility and adaptability, ensuring that the specific conditions of each crop are adequately addressed despite the inherent uncertainties.

4. Feature analysis

This section analyses the variables used in Machine Learning models to better understand how features contribute to model predictions and affect overall model performance. Table 4 presents the Pearson correlation coefficient (PCC) and feature importance score (FIS) for the ET_a model applied to different fields. The features considered include minimum temperature (T_{min}), maximum temperature (T_{max}), dew point temperature (T_{dew}), wind components (U_{wind} and V_{wind}), solar radiation (R_s), and day of the year (DoY). Solar radiation shows a strong positive correlation with ET_a across all fields, with values ranging from 0.63 to 0.79, indicating its predominant influence in the evapotranspiration process. Minimum and maximum temperatures (T_{min} and T_{max}) generally exhibit a positive correlation, though the strength of this correlation varies among the fields, with US-Ne1 showing the highest correlations with T_{min} (0.69) and T_{max} (0.70). Day of the year (DoY) generally shows a low correlation with ET_a, with values ranging from −0.21 to 0.11.

Regarding the feature importance score (FIS), solar radiation (R_s) emerges as the most important feature for most fields, particularly in Villabate (0.81) and CA-ER1 (0.64). Dew point temperature (T_{dew}) shows variable importance, with the highest score in US-ARM (0.10). The wind

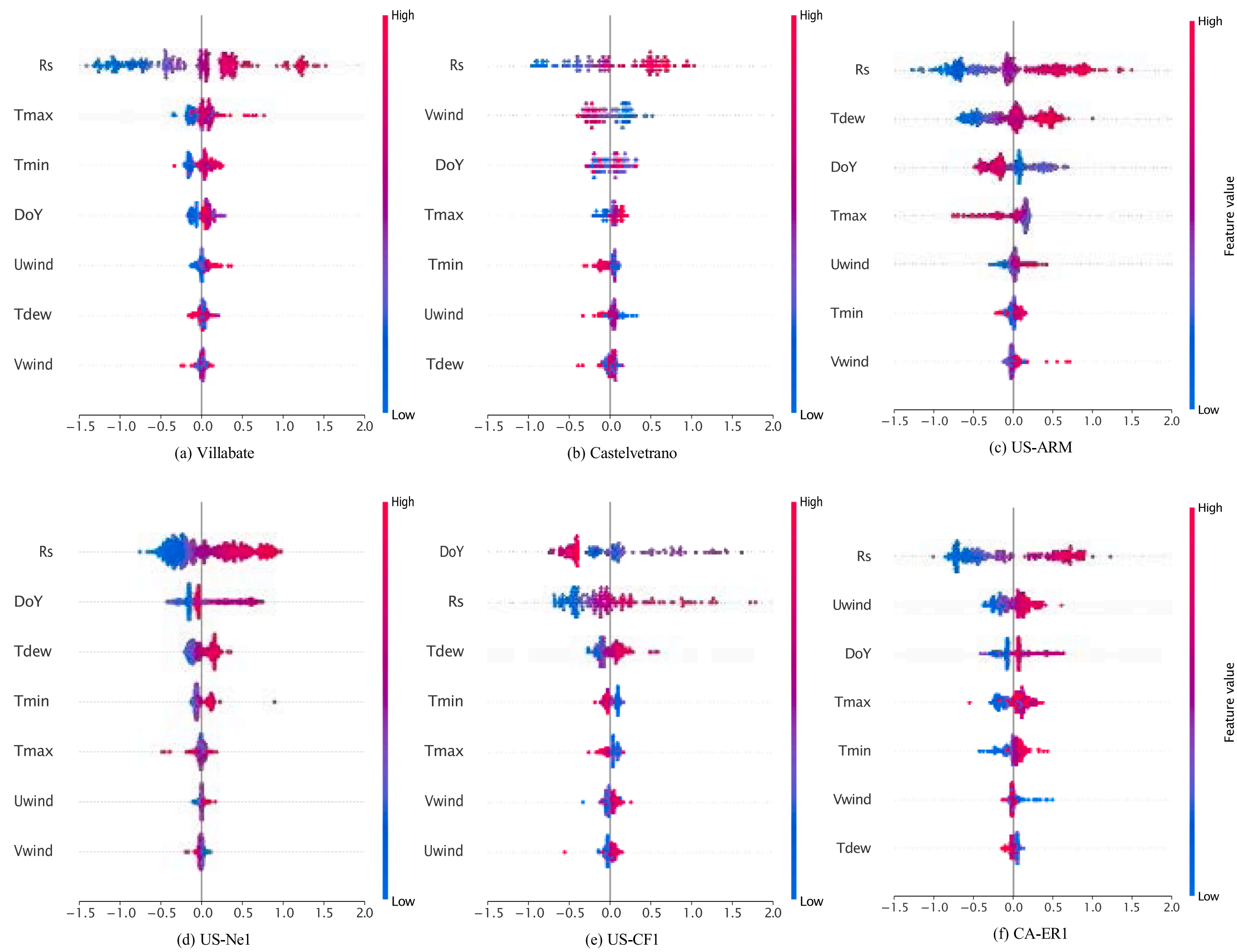

(a) Villabate (b) Castelvetrano (c) US-ARM (d) US-Ne1 (e) US-CF1 (f) CA-ER1

Fig. 3. Shapley Additive Explanations (SHAP) values of the 6 different fields. SHAP values give the impact on ET_a output model for different temperate and continental zones. The higher the absolute SHAP value of the feature, the greater the impact of the feature on the model output, with positive values increasing the output and negative values decreasing the output.

Table 4
Pearson correlation coefficients (PCC) and feature importance scores (FIS) for the data of the different fields.

Score	Field	T_{min}	T_{max}	T_{dew}	U_{wind}	fV_{wind}	R_s	DoY
PCC	Villabate	0.62	0.63	0.53	−0.14	−0.16	0.79	−0.01
	Castelvetrano	0.36	0.45	0.30	0.16	−0.32	0.68	−0.13
	US-ARM	0.41	0.44	0.45	−0.03	0.15	0.63	−0.18
	US-Ne1	0.69	0.70	0.77	−0.16	0.19	0.71	0.07
	US-CF1	0.36	0.39	0.39	0.18	0.02	0.63	−0.21
	CA-ER1	0.57	0.61	0.52	0.13	−0.09	0.68	0.11
FIS	Villabate	0.05	0.04	0.02	0.02	0.01	0.81	0.04
	Castelvetrano	0.02	0.03	0.04	0.04	0.13	0.59	0.13
	US-ARM	0.03	0.06	0.10	0.03	0.03	0.58	0.16
	US-Ne1	0.24	0.19	0.16	0.005	0.003	0.24	0.15
	US-CF1	0.02	0.01	0.03	0.01	0.01	0.48	0.42
	CA-ER1	0.04	0.05	0.02	0.09	0.02	0.64	0.14

component V_{wind} has higher importance scores in Castelvetrano (0.13), while DoY has variable importance scores, with the highest value in US-CF1 (0.42).

The relationship and contribution of each feature to the prediction of ET_a models were investigated using Shapley values based on coalition game theory for each considered climatic zone. Fig. 3 presents the average of the absolute Shapley values for each feature, sorted by decreasing importance. In particular, each point on the graph represents a Shapley value for individual features and variants [44]. The position on the x-axis and y-axis is determined by Shapley values and feature importance, respectively. The color of the points is determined by the feature values, with higher values being more red and lower values being more blue. The swarm plot in Fig. 3 highlights important relationships and shows which features have large positive or large negative SHAP values. For example, solar radiation has the highest mean SHAP value in almost all fields considered, except for the field US-CF1 (Fig. 3e) where, in this case, the DoY has a higher mean SHAP value. In addition, the swarm plot can be used to understand the nature of these relationships for different climatic and continental zones. For example, it is generally observed that as the solar radiation increases, the SHAP value also increases. In contrast, regarding the maximum temperature, an opposite relationship can be seen in some continental zones. Specifically, large values of maximum temperature are associated with smaller negative SHAP values, as can be seen in the case of US-ARM, US-CF1, and US-Ne1 fields.

5. Result and discussion

Table 5 presents a comparison of ET_a predictions obtained through grid search using RF models applied to different geographical areas. Various hyperparameter configurations were tested, including maximum tree depth, minimum samples per leaf, minimum samples per split, and the number of estimators (trees) in the model. Additionally, since the choice of the number of folds in cross-validation can be influenced by the size of the dataset and the complexity of local conditions, for each field

Table 5
Performance comparison of the grid search and ET_a predictions in different fields, using Random Forest (RF) models.

Field	k-folds	Max Depth	Min Samples Leaf	Min Samples Split	Estimators	R^2	RMSE [$mm d^{-1}$]
Villabate	3	10	1	10	100	0.75	0.52
Castelvetrano	4	20	4	2	400	0.64	0.52
US-ARM	4	30	2	2	200	0.65	0.69
US-Ne1	3	10	4	2	300	0.82	0.36
US-CF1	6	20	1	10	100	0.83	0.49
CA-ER1	3	20	1	20	300	0.73	0.52

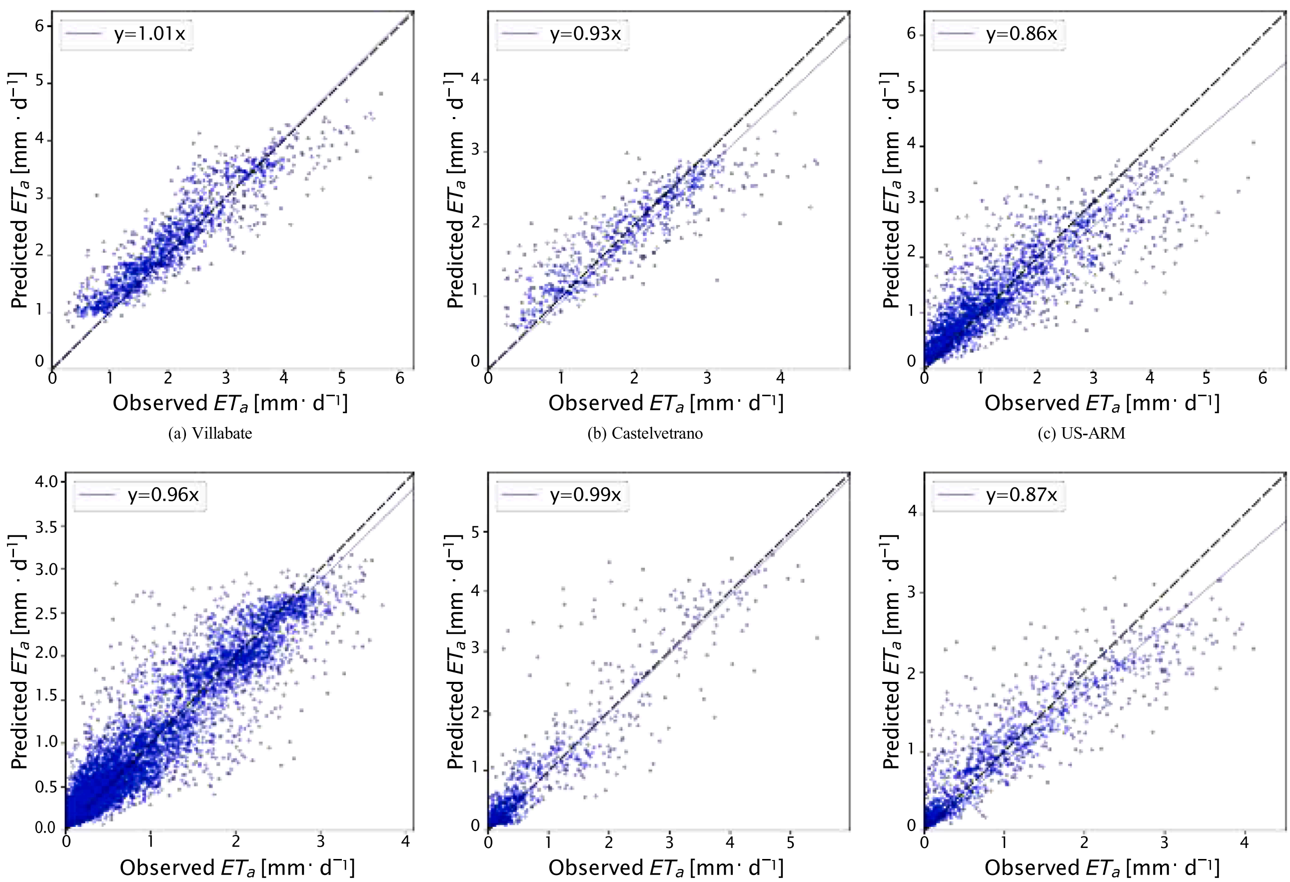

(a) Villabate (b) Castelvetrano (c) US-ARM
(d) US-Ne1 (e) US-CF1 (f) CA-ER1

Fig. 4. Comparison of predicted and observed ET_a values in different fields and climatic zones.

the best k-fold value was empirically determined. The table also shows that the best number of k-folds varies across fields. This variation reflects the need to balance validation accuracy with computational complexity for each specific site. Furthermore, the hyperparameters vary across different fields, reflecting the dimensionality and local variability of the data.

The Table 5 shows that maximum tree depth (Max Depth) ranges from 10 to 30, with fields like US-ARM requiring greater depth to capture more complex relationships, while fields such as Villabate and US-Ne1 use shallower depths to avoid overfitting. The minimum number of samples per leaf (Min Samples Leaf) varies from 1 to 4. In fact, fields with greater local variability, such as US-CF1, adopt a value of 1 to maximise detail, whereas Castelvetrano uses a higher value (4) for increased regularization. The minimum number of samples for a split (Min Samples Split) also varies across fields, with lower values (e.g., 2 in US-ARM and Castelvetrano) allowing more frequent splits, and higher values (10-20) limiting complexity in fields like Villabate and CA-ER1. Lastly, the number of estimators (trees) ranges from 100 to 400, with more complex fields like Castelvetrano requiring a higher number of trees to improve model stability. These differences reflect the specific characteristics of each site and highlight the importance of optimizing models based on local features, balancing model complexity and predictive performance. Finally, the performance of the ET_a prediction models was evaluated using the coefficient of determination R^2 [18] and the root mean square error (RMSE) in $mm\,d^{-1}$ as metrics. Specifically, the Villabate site shows an R^2 of 0.75 and an RMSE of 0.52 $mm\,d^{-1}$, similar results are obtained in the Castelvetrano olive orchard, with an R^2 of 0.64 and an RMSE of 0.52 $mm\,d^{-1}$. The RMSE results obtained for the Italian fields are consistent with those recently reported by [19], who observed minimal differences between variable combinations 4 (only *in situ* meteorological measurements) and 5 (vegetation indices and reanalysis meteorological data). This finding is particularly noteworthy, as it highlights the reliability and applicability of the model developed in this study. Indeed even when using only reanalysis meteorological data, without incorporating vegetation indices, the model achieves performance comparable to approaches that rely on expensive instruments or more complex digital resources. For the American sites, US-Ne1 and US-CF1, the results show good predictions, with R^2 of 0.62 and 0.83, and RMSE values of 0.36 $mm\,d^{-1}$ and 0.49 $mm\,d^{-1}$, respectively. The US-ARM site exhibits an R^2 value of 0.65, accompanied by a RMSE equal to 0.69 $mm\,d^{-1}$. The RMSE values obtained at the American sites are consistent with those reported by [19] with value of RMSE ranging between

Table 6
Comparison of estimated actual crop coefficients during mid-seasons, initial and late seasons in different fields.

	Mid-season stage			Initial and late season stage		
	K_{c-act}	σ	CV [%]	K_{c-act}	σ	CV [%]
Villabate	0.56	0.08	14.3	0.84	0.12	14.3
Castelvetrano	0.42	0.08	19.0	0.70	0.14	20.0
US-ARM	0.28	0.08	28.5	0.50	0.10	20.0
US-Ne1	0.16	0.02	12.5	0.31	0.08	25.8
US-CF1	0.16	0.13	81.2	0.46	0.13	28.2
CA-ER1	0.29	0.10	34.4	0.49	0.15	30.6

0.30 to 0.57 $mm\,d^{-1}$. These results, therefore, further confirm the applicability of the model under different climatic conditions and when using a limited number of input variables. Finally, for the CA-ER1 Canadian site, an R^2 of 0.73 is observed and an RMSE value of 0.52. The performances in terms of RMSE achieved using the framework proposed in this study are consistent with recent works [30,43,88] conducted on different crops and under various climatic conditions, which employ models of varying complexity and a larger number of input variables than those used in this study. In summary, RF models show variable performance in different fields, with the US-Ne1 and US-CF1 sites achieving the best overall accuracy results.

Fig. 4 shows the comparison of the predicted and observed ET_a values in the different fields and climatic zones. From the figure, a difference in the maximum and minimum ET_a values can be observed across the fields. For example, tree crops show higher minimum values compared to herbaceous crops (Villabate 0.2 $mm\,d^{-1}$ and Castelvetrano 0.3 $mm\,d^{-1}$), which have minimums very close to zero. In fact, herbaceous crops (US-ARM, US-CF1, US-Ne1, CA-ER1) show a high density of points in the [0, 1] $mm\,d^{-1}$ range. Instead, the maximum ET_a values ranged from 3.6 $mm\,d^{-1}$ for US-Ne1 to 5.7 $mm\,d^{-1}$ for US-ARM. By comparing the predicted ET_a values with the measured ones, from the identity line it is clear that overestimations occur when the observed ET_a values are below 1 $mm\,d^{-1}$; this is especially noticeable for tree crops, where the phenomenon is more visible compared to herbaceous crops. On the other hand, slight underestimations of ET_a arise for values greater than 3 $mm\,d^{-1}$, particularly in the US-ARM and CA-ER1 fields.

The ET_a values were then used to recover the actual crop coefficient K_{c-act}, as per Eq. 1, along with the reference ET_o obtained via the PM Equation [7]. Separating mid-season and initial/late season stages, Table 6 presents a comparison of the estimated K_{c-act} averaged across the years of observation on the different fields. From the table, it is clear that in the mid-season phase K_{c-act} shows significant variability between sites. For example, Villabate records the highest K_{c-act} value (0.56) with a relatively small standard deviation (0.08) and a coefficient of variation (CV) of 14.3%, indicating a good uniformity in the data. In contrast, US-CF1 has the lowest K_{c-act} value (0.16) and the highest CV (81.2%), showing greater dispersion. Despite the high variability indicated by the CV value, the K_{c-act} for US-CF1, estimated with the proposed framework during the initial and final phenological stages is consistent with that obtained by [89], who used an extensive in situ dataset including leaf area index, meteorological data, and soil moisture measurements. This result confirms that the proposed framework can serve as a valid alternative to costly and time-consuming field measurements.

In the early and late season stage, Villabate maintains the highest values of K_{c-act} (0.84), while US-Ne1 has the lowest value (0.31), with a smaller variability (CV of 25.8%). Overall, the American fields show greater variability than the Italian sites, suggesting significant differences in climatic or management factors that influence crop coefficients.

The estimated values of K_{c-act} for the different fields studied are shown in Figs. 5 and 6. The red line is the trapezoidal reconstruction obtained by averaging the blue dots provided by the framework in the various phenological phases. In particular, Fig. 5a shows that K_{c-act} estimated in the citrus orchard follows a trend similar to the crop coefficient curve reported in the FAO-56 document and Rallo's revised version [7,62]. In particular, high values of K_{c-act} close to 0.84 were obtained from late autumn to early spring, after the beginning of sprouting. Instead, during the irrigation season, under conditions of absent or low rainfall, the estimated K_{c-act} was around 0.56. The analysis in Fig. 5b shows the temporal dynamics of the estimated K_{c-act} in the Castelvetrano olive grove. During the irrigation season (June to September), the average K_{c-act} value was approximately 0.42, closely matching the value reported by [62] ($K_c = 0.45$) for an olive grove with traditional systems (medium plant density).

Fig. 6a illustrates the seasonal variations of K_{c-act} in the US-ARM wheat field. When vegetation was in initial and late season, K_{c-act} averaged 0.50, with peaks reaching up to 0.80. The range of maximum K_{c-act} values aligns with those reported in the literature for vegetation with high cover (e.g., [3,6]). The K_{c-act} decreased during mid-season, particularly between June and December, with an average value of 0.28, closely matching the value proposed by the FAO-56 model (0.25). Fig. 6b shows the estimated K_{c-act} at the US-CF1 site, cultivated with winter wheat, also characterised by seasonal variations. In this case, the crop coefficient values averaged 0.46, with peaks of 0.90 during the early and late seasons (February to June), and values around 0.16 during the mid-season (July to November). The dynamics of the K_{c-act} of maize in the CA-ER1 field are shown in Fig. 6c, with an average minimum value of 0.29 and an average maximum value of 0.49. In addition, two phenological phases within a single year are observed, likely caused by multiple harvests, as reported in [85]. Finally, Fig. 6d shows the dynamics of K_{c-act} for maize in the US-Ne1 field. The reconstructed trapezoid exhibits a maximum value during the initial and final stages of the season, which, averaged over the years, is 0.31, while the minimum value, recorded during the mid-phase of the season, is on average 0.16.

The small differences compared to previous studies can be attributed to the specific conditions and management practices of the fields analysed. Indeed, the FAO provides K_c values based on standard climatic conditions, which assume a sub-humid climate with an average minimum relative humidity of 45% and a moderate wind speed of 2 m/s. However, actual field conditions often differ significantly from these standards, as highlighted in studies [2,32,71].

Table 7 provides a comparative analysis of the performance of the K_{c-act} estimation using various reference methods. The metrics used for this evaluation were presented in Section 2.5. The results indicate that the proposed method provides better predictions in tree orchards when validated against Rallo's baseline method, consistently outperforming the ones achieved using the FAO-56 model as a reference, as evidenced by a lower RMSE (0.073 vs. 0.198) and a PBIAS closer to zero (-0.818 vs. -21.000), in the Villabate field. For Castelvetrano olive orchard, the proposed model showed an RMSE of 0.251 and an nRMSE of 0.076 when validated against the FAO-56 baseline model. Superior performance was observed when the model was cross-validated against Rallo's baseline, achieving an RMSE of 0.143 and an nRMSE of 0.036. In the US-ARM and US-CF1 fields, the proposed method exhibits variable performance compared to the FAO-56 model with frozen soil (fs) and non-frozen soil (nfs) possibilities, with the fs generally delivering better results in terms of RMSE and MBE. When comparing the trapezoid models with the actual crop coefficient values used for testing the ML model, the proposed method generally shows an improved Accuracy Improvement (as defined in Section 2.5). On average, this method significantly enhances accuracy, halving the Root Mean Square Error compared to actual measurements. While the Rallo model performs marginally better, with a negative improvement of about 1%, in the Villabate and Castelvetrano fields, the K_{c-act} values of the reference and proposed models are very close and fall within the acceptable error margins provided. This indicates that in the worst-case scenario, our model is interchangeable with the reference model. Crucially, it provides substantial improvements in other cases, achieving an accuracy gain of up to 83% in the US-Ne1 field.

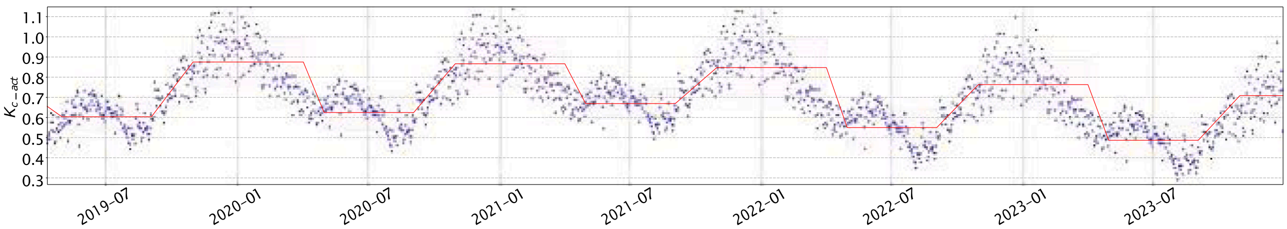

(a) Villabate

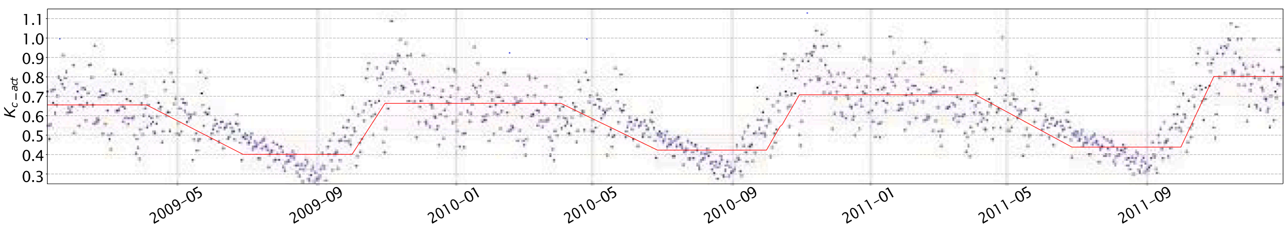

(b) Castelvetrano

Fig. 5. Values of K_{c-act} estimated in the Italian fields of Villabate and Castelvetrano. The points in blue are shown as the scatter plots obtained from the proposed framework. The trapezoidal shape is reconstructed averaging the points in each phenological phase (as given by the two reference FAO-56 papers), where the red line represent the mean and the pink boxes represent the standard deviation of the points with respect to this mean.

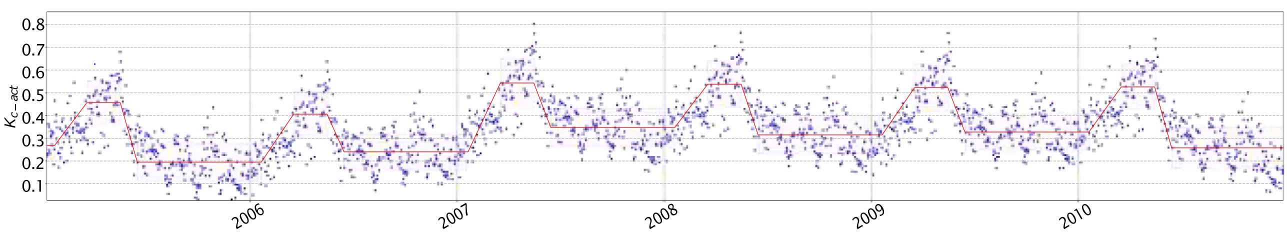

(a) US-ARM

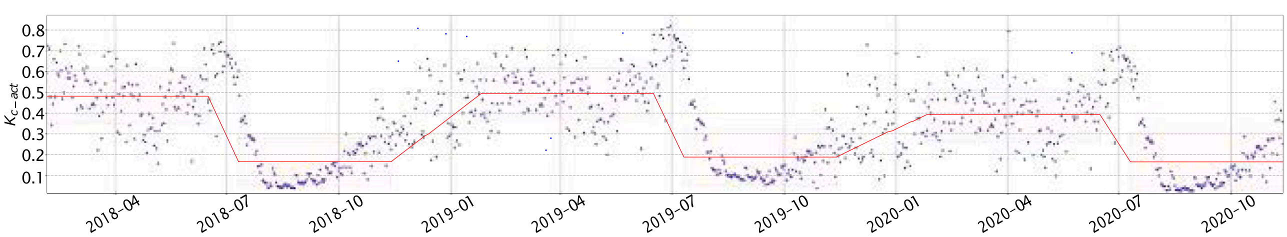

(b) US-CF1

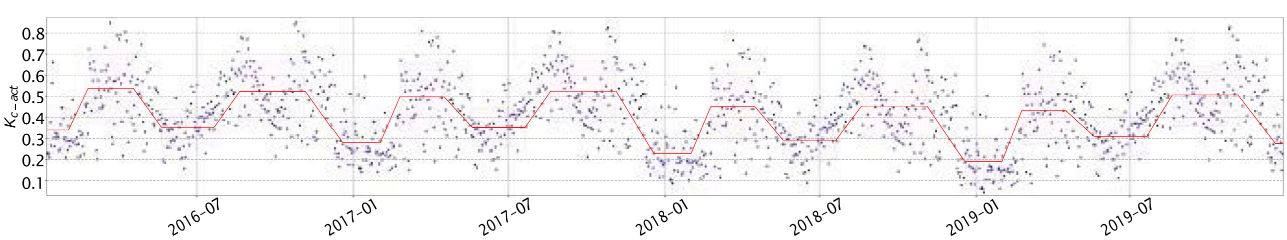

(c) CA-ER1

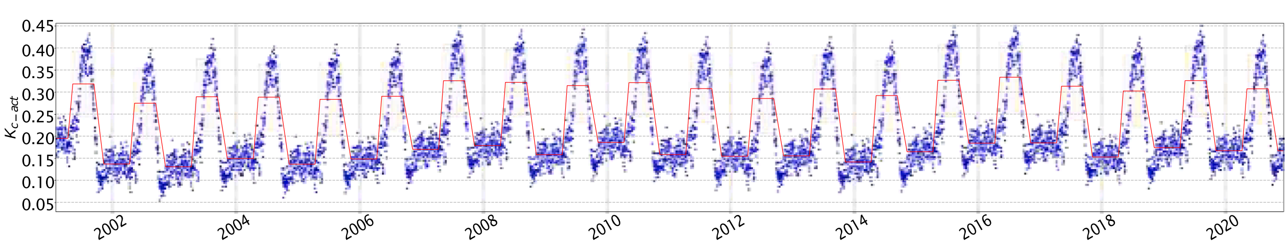

(d) US-Ne1

Fig. 6. Values of K_{c-act} estimated in the American fields of US-ARM, US-CF1, CA-ER1 and US-Ne1. The points in blue represent the scatter-plots obtained from the proposed framework, the red line is the trapezoidal reconstruction and the pink boxes are the standard deviation in the various phenological phases.

Table 7
Performance comparison of K_{c-act} estimation in different fields.

Field	Reference	RMSE	nRMSE	MBE	MAE	PBIAS	Improvement
Villabate	FAO-56	0.198	0.053	0.162	0.450	−21.9	37%
	Rallo	0.073	0.009	0.005	0.281	−0.818	−0.9%
Castelvetrano	FAO-56	0.251	0.076	0.216	0.596	−25.9	45%
	Rallo	0.143	0.036	−0.053	0.068	9.37	−1.2%
US-ARM	FAO-56-fs	0.343	0.235	0.168	0.912	−33.6	49%
	FAO-56-nfs	0.368	0.223	0.276	0.912	−45.4	52%
US-Ne1	FAO-56-mg	0.792	0.678	0.719	1.12	−77.7	83%
	FAO-56-ms	0.750	0.694	0.605	1.12	−74.6	82%
US-CF1	FAO-56-fs	0.509	0.362	0.384	1.05	−53.6	62%
	FAO-56-nfs	0.532	0.359	0.456	1.05	−57.9	64%
CA-ER1	FAO-56-mg	0.561	0.346	0.515	1.12	−56.6	58%
	FAO-56-ms	0.510	0.325	0.405	1.12	−50.6	54%

Table 8
Estimation of water stress coefficients (K_s) values during mid-season, initial and late-season stages across different fields.

Field	Mid-season stage	Initial and late season stage
Villabate	1.00	0.93
Castelvetrano	0.65	0.72
US-ARM	1.00	0.43
US-Ne1	0.64	0.27
US-CF1	0.64	0.38
CA-ER1	0.48	0.41

The proposed framework also allows to estimate the water stress coefficient (K_s) at different growth stages. Table 8 presents the estimated values of K_s during the intermediate, early and late stages of the various fields. These estimates were derived using Eq. (1), where K_s values were calculated by comparing the actual crop coefficient estimates with those tabulated by FAO-56 [7]. This approach provides an indirect indication of potential water stress conditions and allows for a qualitative assessment of model performance under varying environmental conditions, considering the absence of field measurements for validation. The results show the presence of water stress ($K_s < 1$) across all fields and at different growth stages. In the mid-season, CA-ER1 shows the lowest K_s value (0.48), suggesting that water stress is present, while for US-ARM and Villabate ($K_s = 1.00$), no significant water stress is observed during mid-season. For Villabate field, which is very well known in terms of monitoring tools and characteristics, there were only short periods of stress that in this analysis are not evident, due to the averaging over 4 years of observations. The results for the Villabate field are consistent with those obtained by [24,69] and [35] in the same field applying several models to derive the K_s temporal dynamic using *in situ* and remote sensing data. Regarding the K_s values obtained for Castelvetrano, it is possible to note an increase in K_s values, from 0.65 in mid season to 0.72 in early and late season, suggesting a reduction of the field water stress conditions. Moreover, the results are in accordance with those obtained by [20,61] and [34]. The authors of previous studies retrieved, in the same field, the temporal dynamic of K_s using several models and input data from different data sources, supporting the reliability of the results obtained with the proposed framework. Despite this limitation, the results suggest that the estimated K_s values are plausible for the studied sites, reflecting reasonable stress dynamics across different climatic contexts.

During the initial and late stages of the season, K_s values tend to be low overall, indicating the presence of water stress in these stages as well. For example, US-ARM shows a K_s of 0.43 in both the early and late stages of the season. US-Ne1 and US-CF1 show reductions in the two different seasons, with K_s going from 0.64 to 0.27 and from 0.64 to 0.38, respectively, reflecting higher water stress. The results for CA-ER1 field show moderate reductions in K_s across the various seasons, going from 0.48 in mid season to 0.41 in the early and late seasons, suggesting mild to moderate water stress.

In the early growth stages, both wheat [36,40] and maize [5,25] can experience water stress, especially if soil moisture is insufficient. Although wheat has a relatively low water demand during germination and tilling, prolonged drought can hinder root development and tiller formation. Similarly, maize requires less water in its initial vegetative phases compared to flowering and grain filling, but early water deficits can slow growth and reduce the yield potential. However, short periods of water stress can be tolerated if followed by adequate rainfall or irrigation.

Finally, Fig. 7 shows the probability density functions (PDFs) of the noise (or residual) components removed from the K_c effective time series in different fields and climate zones. The noise was computed decomposing the time series in average trend, seasonality, and residual, as described in Section 3.4. From the figure, it is clear that the noise follows a nearly Gaussian distribution, confirming the validity of the proposed methodological approach and supporting the Gaussian hypothesis of the residuals of the analysed data. Furthermore, it is evident that the mean values of noise distributions are generally close to zero, confirming that it is possible to remove the noise residual (thus, focusing only on the trend and seasonal components). The noise variances and standard deviations show slight differences between the fields, with the CA-ER1 field having the greatest variability (Std = 0.197), while Villabate exhibits the least deviation (Std = 0.100). The maximum and minimum values show significant variation among the fields, with Castelvetrano showing the widest range (-0.622 to 0.588), while US-ne1 the narrowest range (-0.338 to 0.399). Despite these differences, the noise distribution across fields appears similar, confirming the robustness of the proposed method and its ability to adapt effectively to different climatic and geographic contexts.

5.1. Limitations and future work

While our framework demonstrates strong potential for optimizing irrigation, its limitations highlight specific directions for future investigation.

In this study, the approach of not using in situ data as model inputs was adopted. This choice ensures good model applicability even in contexts where in situ measurements are not available. On the other hand, the ET_a data measured by EC towers, which are required for model training, are not always accessible, as the instrumentation is expensive and complex to operate. Moreover, in situ instruments for measuring ET_a are particularly sensitive to meteorological and environmental conditions, making them prone to outliers; consequently, the availability of consistent and reliable data series may limit the model's application. Finally, the use of ERA5-L reanalysis climatic data represents a valid alternative in areas where in situ measurements are not feasible; however, the us-

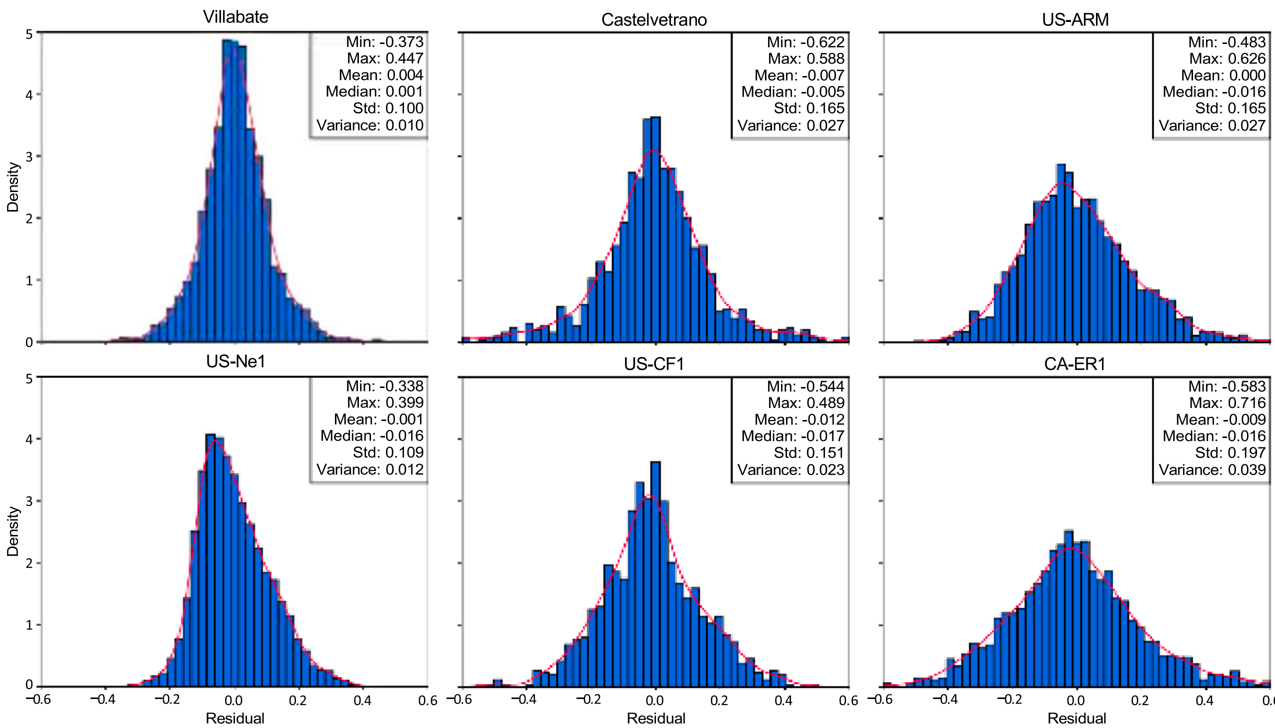

Fig. 7. Probability Density Functions (PDF) of noise removed from K_{c-act} time series across various fields and climatic zones.

ability of these data is restricted to users with adequate computational skills.

Our choice of a Random Forest model, while effective for capturing non-linear interactions, represents one of many possible modelling approaches [52]. We deliberately prioritized a machine learning model that performs well with smaller datasets over more data-intensive deep learning architectures. This approach, however, may not fully capture long-term temporal dependencies within the data. Future investigations could therefore explore recurrent architectures like Long Short-Term Memory (LSTM) networks [4,11] or models incorporating attention mechanisms [80,83]. Such models are adept at identifying time-series correlations and could potentially enhance predictive accuracy, particularly if larger datasets become available. Furthermore, to create a practical and predictable tool for farmers, we adopted certain modelling simplifications. Specifically, our reliance on a naive seasonal decomposition, with additive noise, and generalized FAO reference models may not perfectly account for the unique phenological cycles of specific cultivars or microclimates. This is exemplified by the “Mandarino Tardivo di Ciaculli” in the Villabate field, whose growth cycle is shifted relative to standard varieties. Future iterations of the model could integrate dynamic, field-specific phenological data to create more customized and precise irrigation schedules. As a final consideration for the scalability and cost-effectiveness of our approach, a promising avenue for future work is the application of transfer learning [31,90]. By training a foundational model on a single, sensor-rich “source” field, it could then be fine-tuned for “target” fields with limited or no local measurements. This would drastically lower the barrier to adoption for precision irrigation across multiple, similar agricultural environments.

6. Conclusions

This study proposes a novel method to predict the actual crop coefficient (K_{c-act}) for different crops and climatic zones, using a Random Forest model combined with seasonal decomposition techniques. By integrating ERA5-L reanalysis data with ML techniques, the proposed framework eliminates the need for field sensors, reducing both the costs and maintenance challenges traditionally associated with irrigation monitoring systems. A significant advantage of this framework is that, while it initially requires an Eddy Covariance tower for data acquisition, the farmer is no longer dependent on this instrumentation once the model has been adequately trained. Consequently, the measurement system, with its associated operational complexities, is only necessary for a finite data collection period, after which the tower can be decommissioned or re-deployed to another site. Furthermore, the developed framework is capable of capturing complex relationships between environment and site in temperate and continental zones using reanalysis data. This approach allows farmers to estimate the values of K_{c-act}, optimizing irrigation timing and frequency, improving water use efficiency, and reducing the need for costly field equipment, which involves not only a high initial investment but also periodic maintenance costs. The integration of seasonal decomposition analysis into the model provides an effective tool for estimating K_{c-act} during various phenological stages of crops. The proposed method demonstrated higher performance for tree crops compared to models trained on homogeneous or herbaceous crops. Specifically, the proposed approach achieved an RMSE of 0.143 for an olive orchard and 0.073 for a citrus orchard in the Mediterranean region. This strategy offers farmers a workable way to maximise water use efficiency and strengthen agricultural systems’ resistance to shifting climate conditions, in addition to addressing the problems of data gaps, and avoids the needs of expensive equipment. Finally, these results contribute to the advancement of the United Nations Sustainable Development Goals (SDG), particularly SDG 2 (Zero Hunger), SDG 13 (Climate Action), and SDG 15 (Life on Land), by enabling sustainable water management practices that enhance food security, promote climate-resilient agriculture, and protect terrestrial ecosystems.

CRediT authorship contribution statement

Federico Amato: Writing – original draft, Software, Methodology, Investigation, Formal analysis, Data curation; **Matteo Ippolito:** Writing – original draft, Validation, Methodology, Investigation, Formal analysis, Data curation; **Dario De Caro:** Writing – review & editing, Writing – original draft, Methodology, Investigation, Formal analysis, Data curation; **Daniele Croce:** Writing – review & editing, Supervision, Resources,

Project administration, Funding acquisition; **Antonino Pagano:** Writing – review & editing, Writing – original draft, Software, Project administration, Data curation, Conceptualization.

Data availability

Data will be made available on request.

Declaration of competing interest

The authors declare that they have no known competing financial interests or personal relationships that could have appeared to influence the work reported in this paper.

Acknowledgements

This work was supported by the European Union under the Italian National Recovery and Resilience Plan (NRRP) of NextGenerationEU: partnership on "Telecommunications of the Future" (PE00000001 - program "RESTART"), S2 SUPER - Programmable Networks, Cascade project PRISM - CUP: C79J24000190004; and by project PNRR M4 - C2 - investment 1.1: Projects of Significant National Interest (PRIN) - PRIN 2022 code 2022FYCNPT "IoTSensE: IoT-based Sensing Extension", CUP B53D23002610006.

References

[1] N. Abdennour, T. Ouni, N.B. Amor, The importance of signal pre-processing for machine learning: the influence of data scaling in a driver identity classification, in: 2021 IEEE/ACS 18th International Conference on Computer Systems and Applications (AICCSA), IEEE, 2021, pp. 1–6.

[2] M. Abedinpour, Evaluation of growth-stage-specific crop coefficients of maize using weighing lysimeter, Soil Water Res. 10 (2015).

[3] R. Ahsen, Z. Khan, H. Farid, A. Shakoor, I. Ali, Estimation of cropped area and irrigation water requirement using remote sensing and GIS, J. Anim. Plant Sci. 30 (2020) 876–884.

[4] M. Ali, J.V. Nayahi, E. Abdi, M.A. Ghorbani, F. Mohajeri, A.A. Farooque, S. Alamery, Improving daily reference evapotranspiration forecasts: designing AI-enabled recurrent neural networks based long short-term memory, Ecol. Inf. 85 (2025) 102995.

[5] M.G.B. Allakonon, P.G. Tovihoudji, P.I. Akponikpè, C. Bielders, Optimizing deficit irrigation and fertilizer application for off-season maize production in northern Benin, Field Crops Res. 318 (2024). https://doi.org/10.1016/j.fcr.2024.109613

[6] R.G. Allen, Using the FAO-56 dual crop coefficient method over an irrigated region as part of an evapotranspiration intercomparison study, J. Hydrol. 229 (2000) 27–41.

[7] R.G. Allen, L.S. Pereira, D. Raes, M. Smith, et al., Crop evapotranspiration-guidelines for computing crop water requirements-FAO irrigation and drainage paper 56, 300, Fao, Rome, Fao, Rome, 1998. D05109.

[8] C.S. P.D. Araújo, I.A.C. Silva, M. Ippolito, C.D. G. C.D. Almeida, Evaluation of air temperature estimated by ERA5-land reanalysis using surface data in Pernambuco, Brazil, Environ. Monit. Assess. 194 (2022) 381. https://doi.org/10.1007/s10661-022-10047-2

[9] D. Autovino, M. Minacapilli, G. Provenzano, Modelling bulk surface resistance by MODIS data and assessment of MOD16A2 evapotranspiration product in an irrigation district of Southern Italy, Agric. Water Manag. 167 (2016) 86–94. https://doi.org/10.1016/j.agwat.2016.01.006

[10] D.D. Baldocchi, Assessing the eddy covariance technique for evaluating carbon dioxide exchange rates of ecosystems: past, present and future, Global Change Biol. 9 (2003) 479–492. https://doi.org/10.1046/j.1365-2486.2003.00629.x

[11] M. Bansal, A. Goyal, A. Choudhary, A comparative analysis of k-nearest neighbor, genetic, support vector machine, decision tree, and long short term memory algorithms in machine learning, Decis. Anal. J. 3 (2022) 100071.

[12] S. Biraud, M. Fischer, S. Chan, M. Torn, Ameriflux base US-ARM ARM Southern Great Plains Site- Lamont, Ver. 13-5. Dataset, 2024. https://doi.org/10.17190/AMF/1246027

[13] L. Breiman, Random forests, Mach. Learn. 45 (2001) 5–32.

[14] L. Breiman, J. Friedman, C.J. Stone, R.A. Olshen, Classification and Regression Trees, CRC press, 1984.

[15] C. Cammalleri, M. Anderson, N. Bambach, A. Mcelrone, K. Knipper, M. Roby, G. Ciraolo, D. Decaro, M. Ippolito, C. Corbari, A. Ceppi, M. Mancini, W. Kustas, A fully remote sensing-based implementation of the two-source energy balance model: an application over mediterranean crops, Agric. Water Manag. 306 (2024) 109207. https://doi.org/10.1016/j.agwat.2024.109207

[16] C. Cammalleri, G. Rallo, C. Agnese, G. Ciraolo, M. Minacapilli, G. Provenzano, Combined use of eddy covariance and sap flow techniques for partition of ET fluxes and water stress assessment in an irrigated olive orchard, Agric. Water Manag. 120 (2013) 89–97. https://doi.org/10.1016/j.agwat.2012.10.003.soil

[17] T. Chai, R.R. Draxler, et al., Root mean square error (RMSE) or mean absolute error (MAE), Geosci. Model Dev. Discuss. 7 (2014) 1525–1534.

[18] D. Chicco, M.J. Warrens, G. Jurman, The coefficient of determination R-squared is more informative than SMAPE, MAE, MAPE, MSE and rmse in regression analysis evaluation, Peerj Comput. Scie. 7 (2021) 623.

[19] D.D. Caro, M. Ippolito, M. Cannarozzo, G. Provenzano, G. Ciraolo, Assessing the performance of the gaussian process regression algorithm to fill gaps in the time-series of daily actual evapotranspiration of different crops in temperate and continental zones using ground and remotely sensed data, Agric. Water Manag. 290 (2023). https://doi.org/10.1016/j.agwat.2023.108596

[20] D.D. Caro, M. Ippolito, G. Provenzano, V. Ferro, G. Giordano, S. Orlando, M. Vallone, G. Cascone, S. Porto, Assessing daily ERA5-land reanalysis data to estimate actual evapotranspiration of olive orchards in sicily, in: C. M (Ed.), AIIA 2022: Biosystems Engineering Towards the Green Deal, Cham, Springer International Publishing, 2023, pp. 105–115. https://doi.org/10.1007/978-3-031-30329-6_11

[21] U. Desa/Pop, United nations department of economic and social affairs, population division, Montreal, Canada, Montreal, Canada, 2022. World population prospects 2022: Summary of results.

[22] Er-Raki, Chehbouni, Guemouria, Ezzahar, Khabba, Boulet, Hanich, Citrus orchard evapotranspiration: Comparison between eddy covariance measurements and the FAO-56 approach estimates, Plant Biosyst. 143 (2009) 201–208. https://doi.org/10.1080/11263500802709897

[23] M.L. Fischer, D.P. Billesbach, J.A. Berry, W.J. Riley, M.S. Torn, Spatiotemporal variations in growing season exchanges of CO2, H2O, and sensible heat in agricultural fields of the southern great plains, Earth Interact. 11 (2007) 1–21. https://journals.ametsoc.org/view/journals/eint/11/17/ei231.1.xml. https://doi.org/10.1175/EI231.1

[24] L. Franco, A. Motisi, G. Provenzano, Agro-hydrological models and field measurements to assess the water status of a citrus orchard irrigated with micro-sprinkler and subsurface drip systems, 1314, pp. 75–82. https://doi.org/10.17660/ActaHortic.2021.1314.11

[25] J. Gao, L. Li, R. Ding, S. Kang, T. Du, L. Tong, J. Kang, W. Xu, G. Tang, Grain yield and water productivity of maize under deficit irrigation and salt stress: evidences from field experiment and literatures, Agric. Water Manag. 307 (2025). https://doi.org/10.1016/j.agwat.2024.109260

[26] N. Gorelick, M. Hancher, M. Dixon, S. Ilyushchenko, D. Thau, R. Moore, Google earth engine: planetary-scale geospatial analysis for everyone, Remote Sens. Environ. 202 (2017) 18–27. Big Remotely Sensed Data: tools, applications and experiences, https://doi.org/10.1016/j.rse.2017.06.031

[27] N. Gourgouletis, M. Gkavrou, E. Baltas, Comparison of empirical ETo relationships with ERA5-land and in situ data in Greece, Geographies 3 (2023) 499–521. https://www.mdpi.com/2673-7086/3/3/26. https://doi.org/10.3390/geographies3030026

[28] F. Granata, Evapotranspiration evaluation models based on machine learning algorithms-a comparative study, Agric. Water Manag. 217 (2019) 303–315.

[29] F. Granata, R. Gargano, G.D. Marinis, Artificial intelligence based approaches to evaluate actual evapotranspiration in wetlands, Sci. Total Environ. 703 (2020) 135653.

[30] Y. Hao, J. Baik, H. Tran, M. Choi, Quantification of the effect of hydrological drivers on actual evapotranspiration using the Bayesian model averaging approach for various landscapes over Northeast Asia, J. Hydrol. 607 (2022). https://doi.org/10.1016/j.jhydrol.2022.127543

[31] A. Hosna, E. Merry, J. Gyalmo, Z. Alom, Z. Aung, M.A. Azim, Transfer learning: a friendly introduction, J. Big Data 9 (2022) 102.

[32] K. Igwe, V. Sharda, T. Hefley, Evaluating the impact of future seasonal climate extremes on crop evapotranspiration of maize in Western Kansas using a machine learning approach, 12, 2023.

[33] M. Ippolito, D.D. Caro, M. Cannarozzo, G. Provenzano, G. Ciraolo, Evaluation of daily crop reference evapotranspiration and sensitivity analysis of FAO Penman-Monteith equation using ERA5-land reanalysis database in Sicily, Italy, Agric. Water Manag. 295 (2024) 108732. https://doi.org/10.1016/j.agwat.2024.108732

[34] M. Ippolito, D.D. Caro, F. Capodici, G. Ciraolo, Distributed FAO56 agro-hydrological model for irrigation scheduling in olives orchards, 2023. https://doi.org/10.1109/MetroAgriFor58484.2023.10424381

[35] M. Ippolito, D.D. Caro, G. Ciraolo, M. Minacapilli, G. Provenzano, Estimating crop coefficients and actual evapotranspiration in citrus orchards with sporadic cover weeds based on ground and remote sensing data, 2022, pp. 1–18.

[36] N. Jin, W. Ren, B. Tao, L. He, Q. Ren, S. Li, Q. Yu, Effects of water stress on water use efficiency of irrigated and rainfed wheat in the loess plateau, china, Sci. Total Environ. 642 (2018) 1–11. https://doi.org/10.1016/j.scitotenv.2018.06.028

[37] J.C. Kaimal, J.J. Finnigan, Atmospheric Boundary Layer Flows: Their Structure and Measurement, Oxford University Press, 1994. https://doi.org/10.1093/oso/9780195062397.001.0001

[38] R. Kohavi, et al., A study of cross-validation and bootstrap for accuracy estimation and model selection, in: IJCAI, 1995, pp. 1137–1145.

[39] M. Kottek, J. Grieser, C. Beck, B. Rudolf, F. Rubel, World map of the köppen-Geiger climate classification updated, Meteorologische Zeitschrift 15 (2006) 259–263. https://doi.org/10.1127/0941?2948/2006/0130

[40] A. Kumari, D. Singh, A. Sarangi, M. Hasan, V.K. Sehgal, Optimizing wheat supplementary irrigation: Integrating soil stress and crop water stress index for smart scheduling, in: Agricultural Water Management 305, 109104, 2024. https://doi.org/10.1016/j.agwat.2024.109104

[41] W.P. Kustas, J.H. Prueger, K.S. Humes, P.J. Starks, Estimation of surface heat fluxes at field scale using surface layer versus mixed-layer atmospheric variables with radiometric temperature observations, J. Appl. Meteorol. 38 (1999) 224–238.

[42] F.T. Liu, K.M. Ting, Z.H. Zhou, Isolation forest, in: 2008 Eighth IEEE International Conference on Data Mining, IEEE, 2008, pp. 413–422.

[43] J. Liu, X. Meng, Y. Ma, X. Liu, Introduce canopy temperature to evaluate actual evapotranspiration of green peppers using optimized ENN models, J. Hydrol. 590 (2020). https://doi.org/10.1016/j.jhydrol.2020.125437

[44] S.M. Lundberg, S.I. Lee, I. Guyon, U.V. Luxburg, S. Bengio, H. Wallach, R. Fergus, S. Vishwanathan, A unified approach to interpreting model predictions, in: R. Garnett (Ed.), Advances in Neural Information Processing Systems 30, Curran Associates, Inc, 2017, pp. 4765–4774. http://papers.nips.cc/paper/7062-a-unified-approach-to-interpreting-model-predictions.pdf.

[45] G. Manca, Analisi dei flussi di carbonio di una cronosequenza di cerro (quercus cerris l.) dell'italia centrale attraverso la tecnica della correlazione turbolenta, Technical Report, University of Tuscia, Viterbo, 2003.

[46] M. Mauder, T. Foken, R. Clement, J.A. Elbers, W. Eugster, T. Grünwald, B. Heusinkveld, O. Kolle, Quality control of carboeurope flux data; part 2: Inter-comparison of eddy-covariance software, Biogeosciences 5 (2008) 451–462. https://bg.copernicus.org/articles/5/451/2008/. https://doi.org/10.5194/bg-5-451-2008

[47] D. Menefee, R.L. Scott, M. Abraha, J. Alfieri, J. Baker, D.M. Browning, J. Chen, J. Gonet, J. Johnson, G. Miller, R. Nifong, P. Robertson, E. Russell, N. Saliendra, A.P. Schreiner-Mcgraw, A. Suyker, P. Wagle, C. Wente, P. White, D. Smith, Unraveling the effects of management and climate on carbon fluxes of U.S. croplands using the usda long-term agroecosystem (LTAR) network, Agric. Forest Meteorol. 326 (2022) 109154. https://doi.org/10.1016/j.agrformet.2022.109154

[48] J. Moncrieff, J. Massheder, H.D. Bruin, J. Elbers, T. Friborg, B. Heusinkveld, P. Kabat, S. Scott, H. Soegaard, A. Verhoef, A system to measure surface fluxes of momentum, sensible heat, water vapour and carbon dioxide, J. Hydrol. 188 (189) (1997) 589–611. https://doi.org/10.1016/S0022-1694(96)03194-0.hAPEX-Sahel

[49] D.N. Moriasi, J.G. Arnold, M.W.V. Liew, R.L. Bingner, R.D. Harmel, T.L. Veith, Model evaluation guidelines for systematic quantification of accuracy in watershed simulations, Trans. ASABE 50 (2007) 885–900.

[50] A. Negm, J. Jabro, G. Provenzano, Assessing the suitability of american national aeronautics and space administration (NASA) agro-climatology archive to predict daily meteorological variables and reference evapotranspiration in Sicily, Italy, Agric. Forest Meteorol., 2017 244-245. https://doi.org/10.1016/j.agrformet.2017.05.022

[51] A. Pagano, F. Amato, M. Ippolito, D.D. Caro, D. Croce, A machine learning framework to estimate crop coefficient dynamics of citrus orchards, Comput. Electron. Agric. 238 (2025) 110797.

[52] A. Pagano, F. Amato, M. Ippolito, D.D. Caro, D. Croce, A. Motisi, G. Provenzano, I. Tinnirello, Machine learning models to predict daily actual evapotranspiration of citrus orchards under regulated deficit irrigation, Ecol. Inf. 76 (2023) 102133.

[53] W.S. Parker, Reanalyses and observations: What's the difference?, Bull. Am. Meteorol. Soc. 97 (2016) 1565–1572. https://journals.ametsoc.org/view/journals/bams/97/9/bams-d-14-00226.1.xml. https://doi.org/10.1175/BAMS-D-14-00226.1

[54] G. Pastorello, D. Agarwal, D. Papale, T. Samak, C. Trotta, A. Ribeca, C. Poindexter, B. Faybishenko, D. Gunter, R. Hollowgrass, E. Canfora, Observational data patterns for time series data quality assessment, in: IEEE 10th International Conference on e-Science, 2014, pp. 271–278. https://doi.org/10.1109/eScience.2014.45

[55] G. Pastorello, C. Trotta, E. Canfora, et al., The fluxnet2015 dataset and the oneflux processing pipeline for eddy covariance data, in: Scientific Data 7, 2020, p. 225. https://doi.org/10.1038/s41597-020-0534-3

[56] A. Pelosi, Performance of the copernicus european regional reanalysis (CERRA) dataset as proxy of ground-based agrometeorological data, Agric. Water Manag. 289 (2023). https://doi.org/10.1016/j.agwat.2023.108556

[57] A. Pelosi, G. Chirico, Regional assessment of daily reference evapotranspiration: can ground observations be replaced by blending ERA5-land meteorological reanalysis and CM-SAF satellite-based radiation data?, Agric. Water Manag. 258 (2021) 107169. https://doi.org/10.1016/j.agwat.2021.107169

[58] A. Pelosi, F. Terribile, G. D'urso, G.B. Chirico, Comparison of ERA5-land and UERRA MESCAN-SURFEX reanalysis data with spatially interpolated weather observations for the regional assessment of reference evapotranspiration, Water 12 (2020). https://www.mdpi.com/2073-4441/12/6/1669. https://doi.org/10.3390/w12061669

[59] C.L. Phillips, D. Huggins, AmeriFlux BASE US-CF1 CAF-LTAR Cook East Ver. 3-5. Dataset, 2022. https://doi.org/10.17190/AMF/1543382

[60] J. Prueger, J. Hatfield, T. Parkin, W. Kustas, L. Hipps, C. Neale, J. Macpherson, W. Eichinger, D. Cooper, Tower and aircraft eddy covariance measurements of water vapor, energy, and carbon dioxide fluxes during smacex, J. Hydrometeorol. 6 (2005) 954–960.

[61] A. Puig-Sirera, G. Rallo, P. Paredes, T.A. Paço, M. Minacapilli, G. Provenzano, L.S. Pereira, Transpiration and water use of an irrigated traditional olive grove with sap-flow observations and the FAO56 dual crop coefficient approach, Water 13 (2021). https://www.mdpi.com/2073-4441/13/18/2466. https://doi.org/10.3390/w13182466

[62] G. Rallo, T. Paço, P. Paredes, A. Puig-Sirera, R. Massai, G. Provenzano, L. Pereira, Updated single and dual crop coefficients for tree and vine fruit crops, Agric. Water Manag. 250 (2021) 106645.

[63] G. Rallo, G. Provenzano, Modelling eco-physiological response of table olive trees (Olea europaea L.) to soil water deficit conditions, Irrig. Sustain. Pract. 120 (2013) 79–88. https://doi.org/10.1016/j.agwat.2012.10.005.soil

[64] N. Raz-Yaseef, D.P. Billesbach, M.L. Fischer, S.C. Biraud, S.A. Gunter, J.A. Bradford, M.S. Torn, Vulnerability of crops and native grasses to summer drying in the u.s. southern great plains, Agric. Ecosyst. Environ. 213 (2015) 209–218. https://doi.org/10.1016/j.agee.2015.07.021

[65] N.J. Rosenberg, B.L. Blad, S.B. Verma, Microclimate: The Biological Environment, John Wiley & Sons, 1983.

[66] J.M. noz Sabater, E. Dutra, A.A. Panareda, C. Albergel, G. Arduini, G. Balsamo, S. Boussetta, M. Choulga, S. Harrigan, H. Hersbach, B. Martens, D.G. Miralles, M. Piles, N.J.R. ǵuez Fernández, E. Zsoter, C. Buontempo, J.N. Thépaut, ERA5-land: a state-of-the-art global reanalysis dataset for land applications, Earth Syst. Sci. Data 13 (2021) 4349–4383. https://essd.copernicus.org/articles/13/4349/2021/, https://doi.org/10.5194/essd-13-4349-2021.

[67] F. Schrader, W. Durner, J. Fank, S. Gebler, T. Pütz, M. Hannes, U. Wollschläger, Estimating precipitation and actual evapotranspiration from precision lysimeter measurements, four Decades of Progress in Monitoring and Modeling of Processes in the Soil-Plant-Atmosphere System: Applications and Challenges 19 (2013) 543–552. https://doi.org/10.1016/j.proenv.2013.06.061

[68] S. Seabold, J. Perktold, Statsmodels: Econometric and statistical modeling with python, in: Proceedings of the 9th Python in Science Conference, the 9th Python in Science ConferenceAustin, TX, 2010, pp. 10–25080.

[69] D.A. Segovia-Cardozo, L. Franco, G. Provenzano, Detecting crop water requirement indicators in irrigated agroecosystems from soil water content profiles: An application for a citrus orchard, Sci. Total Environ. 806 (2022) 150492.

[70] J. Sheffield, A.D. Ziegler, E.F. Wood, Y. Chen, Correction of the high-latitude rain day anomaly in the NCEP-NCAR reanalysis for land surface hydrological modeling, J. Clim. 17 (2004) 3814–3828. https://journals.ametsoc.org/view/journals/clim/17/19/1520-0442_2004_017_3814_cothrd_2.0.co_2.xml. https://doi.org/10.1175/1520-0442(2004)017 < 3814:COTHRD > 2.0.CO;2

[71] R.K. Singh, A. Irmak, Estimation of crop coefficients using satellite remote sensing, J. Irrig. Drainage Eng. 135 (2009) 597–608.

[72] P. Steduto, T.C. Hsiao, D. Raes, E. Fereres, Aquacropâ€ the FAO crop model to simulate yield response to water: I. Concepts and underlying principles, Agronomy J. 101 (2009) 426–437. https://doi.org/10.2134/agronj2008.0139s

[73] R.B. Stull, An Introduction to Boundary Layer Meteorology, Springer Science & Business Media 13, 1988.

[74] A. Suyker, Ameriflux base us-ne1 mead - irrigated continuous maize site, 2024. https://doi.org/10.17190/AMF/1246084

[75] A. Suyker, S. Verma, G. Burba, T. Arkebauer, D. Walters, K. Hubbard, Growing season carbon dioxide exchange in irrigated and rainfed maize, Agric. Forest Meteorol. 124 (2004) 1–13. https://doi.org/10.1016/j.agrformet.2004.01.011

[76] T.E. Twine, W. Kustas, J. Norman, D. Cook, P. Houser, T. Meyers, J. Prueger, P. Starks, M. Wesely, Correcting eddy-covariance flux underestimates over a grassland, Agric. Forest Meteorol. 103 (2000) 279–300.

[77] United nations, the united nations world water development report 2021: Valuing water, UNESCO, 2021. Unesco, Paris.

[78] S.V. Buuren, K. Groothuis-Oudshoorn, mice: Multivariate imputation by chained equations in R, J. Stat. Softw. 45 (2011) 1–67.

[79] D. Vanella, G. Longo-Minnolo, O.R. Belfiore, J.M. Ramírez-Cuesta, S. Pappalardo, S. Consoli, G. D'urso, G.B. Chirico, A. Coppola, A. Comegna, A. Toscano, R. Quarta, G. Provenzano, M. Ippolito, A. Castagna, C. Gandolfi, Comparing the use of ERA5 reanalysis dataset and ground-based agrometeorological data under different climates and topography in Italy, J. Hydrol. Reg. Stud. 42 (2022). https://doi.org/10.1016/j.ejrh.2022.101182

[80] A. Vaswani, N. Shazeer, N. Parmar, J. Uszkoreit, L. Jones, A.N. Gomez, L. Kaiser, I. Polosukhin, Attention is all you need. Adv. Neural Inf. Process. Syst., 30 (2017.

[81] Vesala, W. Eugster, A. Ojala, Eddy covariance: a practical guide to measurement and data analysis, Springer Atmos. Sci. Ser. 12 (2012) 365–376. https://doi.org/10.1007/978-94-007-2351-1

[82] C. Wagner-Riddle, Ameriflux base CA-ER1 Elora Research Station, Ver. 3-5. Dataset, 2021. https://doi.org/10.17190/AMF/1579541

[83] S. Wang, X. Yu, Y. Li, S. Wang, C. Meng, Application of a hybrid deep learning approach with attention mechanism for evapotranspiration prediction: a case study from the mount Tai Region, China, Earth Science Informatics 16 (2023) 3469–3487.

[84] C.J. Willmott, K. Matsuura, Advantages of the mean absolute error (MAE) over the root mean square error (RMSE) in assessing average model performance, Clim. Res. 30 (2005) 79–82.

[85] D.A. Wood, Net ecosystem exchange comparative analysis of the relative influence of recorded variables in well monitored ecosystems, Ecol. Complexity 50 (2022) 100998.

[86] Z. Xu, S. Liu, M. Hu, Measurements of evapotranspiration by eddy covariance system in the Hai River Basin, in: Proceedings of the 2009 International Symposium of HAIHE Basin Integrated Water and Environment Management, the 2009 International Symposium of HAIHE Basin Integrated Water and Environment Management-Beijing, China, 2009.

[87] J. Yang, J.Y. Yang, S. Liu, G. Hoogenboom, An evaluation of the statistical methods for testing the performance of crop models with observed data, Agric. Syst. 127 (2014) 81–89.

[88] C. Zhang, G. Luo, O. Hellwich, C. Chen, W. Zhang, M. Xie, H. He, H. Shi, Y. Wang, A framework for estimating actual evapotranspiration at weather stations without flux observations by combining data from modis and flux towers through a machine learning approach, J. Hydrol. 603 (2021). https://doi.org/10.1016/j.jhydrol.2021.127047

[89] X. Zhang, S. Chen, H. Sun, L. Shao, Y. Wang, Changes in evapotranspiration over irrigated winter wheat and maize in North China plain over three decades, Agric. Water Manag. 98 (2011) 1097–1104. https://doi.org/10.1016/j.agwat.2011.02.003

[90] Z. Zhao, L. Alzubaidi, J. Zhang, Y. Duan, Y. Gu, A comparison review of transfer learning and self-supervised learning: definitions, applications, advantages and limitations, Expert Syst. Appl. 242 (2024) 122807.